Probing Molecular Relaxation on Polymer Surfaces with Friction Force Microscopy

Greg Haugstad*

Center for Interfacial Engineering, University of Minnesota, 187 Shepherd Laboratories, Minneapolis, Minnesota 55455

Wayne L. Gladfelter*

Department of Chemistry, University of Minnesota, Minneapolis, Minnesota 55455

Elizabeth B. Weberg, Rolf T. Weberg, and Richard R. Jones

Medical Products Division, E. I. du Pont de Nemours and Co., Staton Road, Brevard, North Carolina 28712

Received January 23, 1995. In Final Form: May 24, 1995®

The scan-velocity dependence of friction force microscopy (FFM) is characterized on gelatin films and related to the rate dependence of molecular relaxations. For selected scanning-parameter values the velocity dependence of frictional force is affected by the measurement process, because of energy imparted to the tip–sample contact region: a peak in the friction–velocity relationship, attributed to the glass-to-rubber transition, shifts to higher velocity for increasingly-perturbative scanning. Subsequent imaging at less perturbative scanning conditions reveals residual elevated frictional forces, but no corresponding morphological changes, in the perturbed regions. This is attributed to greater relaxational dissipation of energy from higher-energy molecular conformations attained in the rubbery state. Relaxation to lower-energy conformations in turn leaves the scanned region exhibiting lower frictional forces, i.e., in a less dissipative state characteristic of the scanning conditions during repeated imaging. The ability to image variations in frictional dissipation tens of nanometers in lateral size is demonstrated. These variations are sampled statistically over micrometer-scale regions to yield "friction spectroscopy" histograms, i.e., number of image pixels versus frictional force. Histogram breadth and symmetry apparently reflect the energy dispersion of relaxations characteristic of glassy or rubbery behavior. The fundamental understandings of FFM derived in this study are applied to assess crystallinity and aging in gelatin films.

1. Introduction

Scanning force microscopy (SFM) has emerged as a premier tool to image many classes of materials of scientific and technological interest. The additional capacity of SFM to investigate a staggering array of material *properties* derives from its ability to probe interactions ranging from the simple to the complex: Pauli exclusion, Coulomb, magnetic, van der Waals, adhesive, frictional, and specific biological.[1–9] Several SFM studies have demonstrated a great sensitivity to friction on organic materials;[7,8,10–19] not surprisingly, much of this work has focused on materials relevant to lubrication. Of more general interest is the finding that friction force microscopy (FFM) can distinguish dissimilar materials[7,8,10–15] and delineate anisotropies in crystalline films.[13,17] Our recent study of thin gelatin films on mica showcased the ability of FFM to distinguish biopolymer phases differing in dissipative character, and to do so diagnostically vis-a-vis a phase-specific coefficient of friction.[7]

In continuing work we are striving to develop a molecular-scale understanding of the energy dissipation manifest in FFM of polymer films. Friction on polymers has a large, even dominant, contribution from internal viscoelastic dissipation which ultimately derives from molecular relaxation; traditionally this has been characterized in macroscopic measurements of frictional force as a function of velocity.[20,21] In the present FFM study we investigate the scan-velocity dependence of friction on

® Abstract published in *Advance ACS Abstracts,* August 15, 1995.

(1) Hues, S. M.; Colton, R. J.; Meyer, E.; Guntherodt, H. *MRS Bull.* **1993**, *18* (1), 41–49.
(2) Overney, R.; Meyer, E. *MRS Bull.* **1993**, *18* (5), 26–34.
(3) Hartmann, U.; Goddenhenrich, T.; Heiden, C. *J. Magn. Magn. Mater.* **1991**, *101*, 263–270.
(4) Burnham, N. A.; Dominguez, D. D.; Mowery, R. L.; Colton, R. J. *Phys. Rev. Lett.* **1990**, *64*, 1931–1934.
(5) Blackman, G. S.; Mate, C. M.; Philpott, M. R. *Phys. Rev. Lett.* **1990**, *65*, 2270–2273.
(6) Weisenhorn, A. L.; Maivold, P.; Butt, H.; Hansma, P. K. *Phys. Rev. B* **1992**, *45*, 11226–11232.
(7) Haugstad, G.; Gladfelter, W. L.; Weberg, E. B.; Weberg, R. T.; Weatherill, T. D. *Langmuir* **1994**, *10*, 4295–4306.
(8) Frisbie, C. D.; Rozsnyai, L. F.; Noy, A.; Wrighton, M. S.; Lieber, C. M. *Science* **1994**, *265*, 2071–2074.
(9) Florin, E.; Moy, V. T.; Gaub, H. E. *Science* **1994**, *264*, 415–417.
(10) Meyer, E.; Overney, R.; Brodbeck, D.; Howald, L.; Luthi, R.; Frommer, J.; Guntherodt, H. *Phys. Rev. Lett.* **1992**, *69*, 1777.
(11) Meyer, E.; Overney, R.; Lüthi, R.; Brodbeck, D.; Howald, L.; Frommer, J.; Güntherodt, H.; Wolter, O.; Fujihira, M.; Takano, H.; Gotoh, Y. *Thin Solid Films* **1992**, *220*, 132–137.
(12) Overney, R. M.; Meyer, E.; Frommer, J.; Brodbeck, D.; Lüthi, R.; Howald, L.; Güntherodt, H.; Fujihira, M.; Takano, H.; Gotoh, Y. *Nature* **1992**, *359*, 133–135.
(13) Overney, R. M.; Takano, H.; Fujihira, M.; Paulus, W.; Ringsdorf, H. *Phys. Rev. Lett.* **1994**, *72*, 3546–3549.
(14) Overney, R. M.; Meyer, E.; Frommer, J.; Güntherodt, H.; Fujihira, M.; Takano, H.; Gotoh, Y. *Langmuir* **1994**, *10*, 1281–1286.
(15) Haugstad, G.; Gladfelter, W. L.; Weberg, E. B. *Langmuir* **1993**, *9*, 3717–3721.
(16) Mate, C. M. *Phys. Rev. Lett.* **1992**, *68*, 3323–3326.
(17) Nisman, R.; Smith, P.; Vancso, G. J. *Langmuir* **1994**, *10*, 1667–1669.
(18) Liu, Y.; T., W.; Evans, D. F. *Langmuir* **1994**, *10*, 2241–2245.
(19) O'Shea, S. J.; Welland, M. E.; Rayment, T. *Langmuir* **1993**, *9*, 1826–1835.
(20) *Advances in Polymer Friction and Wear*; Lee, L., Ed.; Plenum Press: New York, 1974; Vol. 5.
(21) Moore, D. F. *The Friction and Lubrication of Elastomers*; Pergamon Press, Ltd.: Oxford, 1972; p 288.

0743-7463/95/2411-3473$09.00/0

gelatin to probe molecular relaxation. In technological gelatin films this relaxation should depend strongly on the nature and extent of cross-linking,[22] including the role of extrinsic coupling agents. These issues are of keen interest to many engaged in research and development in the photographic and other industries.[23] The focus of the present article, however, is on the *methodology* we have developed to collect, process, and interpret FFM data on gelatin, procedures applicable to studies of polymeric and other organic films in general.

We find that for select scanning conditions the velocity dependence of frictional force can be affected by the measurement process, because of energy imparted to the tip–sample contact region. This has residual effects on the frictional characteristics, but not on the imaged morphology, of the "perturbed" region. Unique strengths of FFM are featured in the ability to image the effects of perturbative measurements and to resolve lateral variations in frictional dissipation. We present the first application of FFM to probe the dispersion of relaxational dissipation in "friction spectroscopy", i.e., histograms of the frictional forces measured across a surface region. The dispersion and mean value of frictional forces differ markedly for glassy versus rubbery film behavior. Interpretations in terms of molecular conformation are discussed.

2. Experimental Details

Aqueous gelatin solutions of 10^{-3} to 1 wt % were prepared by slowly heating (≈2 h) a 1 wt % mixture of gelatin (Kind and Knox photographic grade, type 2688) in distilled/deionized water (DW) to ≈45 °C, followed by dilution with DW at 20 °C to the desired concentration. Freshly-cleaved muscovite mica (Union Mica Corp.) substrates were rinsed in DW, immersed in the aqueous gelatin solution (at least 2 h old initially) for 3 h, rinsed in a DW bath, carefully extracted to retain a residual puddle of water, covered, and allowed to dry slowly overnight at 20 °C in moderate-humidity (30% < RH < 60%) conditions. The films were initially imaged in air the following day. Repeated imaging over a period of weeks or months (depending on the sample) reproduced the same film morphology. Results discussed below are qualitatively characteristic of all films investigated (≈25), independent of the concentration of the solution from which they were prepared. Quantitative differences between films prepared from high- and low-concentration solutions will be discussed in another article.

The Nanoscope III (Digital Instruments) SFM was used for all film characterization. We employed the 1231J scanner with lateral/vertical scanning ranges of 150/4.7 μm and commercial triangular 100-μm cantilevers (spring constant = 0.58 N/m) with integrated Si_3N_4 tips. Topographic and frictional force (F_f) images were simultaneously collected at constant vertical cantilever deflection; the total load or "contact force" (F_c) was controllably in the 20–200 nN range as indicated in the text (with the exception of Figure 2 as explained below). Images were collected with the tip scanning left-to-right in the sample's inertial frame. Friction-actuated cantilever torsion was enabled by choosing a fast-scan direction perpendicular to the primary cantilever axis.

"Friction loop" data were collected in the "y-disabled" mode, where scanning is performed along the fast (x), but not the slow (y), scanning axis. An example of the raw data is illustrated in Figure 1, a plot of the lateral force measured on nominally-dry gelatin as a function of the tip position for a single left-to-right/right-to-left cycle. Frictional force, being nonconservative, was quantified as the difference of the average lateral force sensed (including sign) while scanning in opposite directions (equivalent to evaluating a closed path integral). The data at the extreme left and right ends of the scanning interval (outside of the vertical lines) correspond to the static friction region, where the tip has not yet attained a sliding state.[2] Our quantification of frictional force ignores these data in order to characterize only the sliding friction (between the vertical lines). Presently we are interested only in the *relative* frictional force at different scan velocities or contact forces, so we quantify it as the voltage measured at the cantilever-torsion sensing photodetector,[2] or simply in "relative units". The reader interested in the evaluation of absolute frictional force is referred to published work by us[7,15] and others.[2,18]

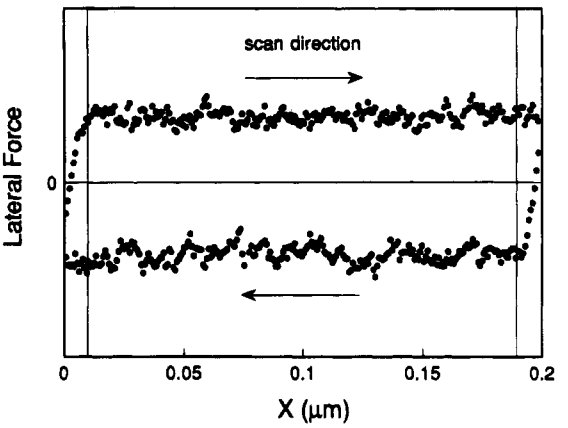

Figure 1. Lateral force measured on gelatin as a function of the tip position for a single left-to-right/right-to-left cycle. The data at the extreme left and right ends of the scanning interval (outside of the vertical lines) correspond to the static friction region.

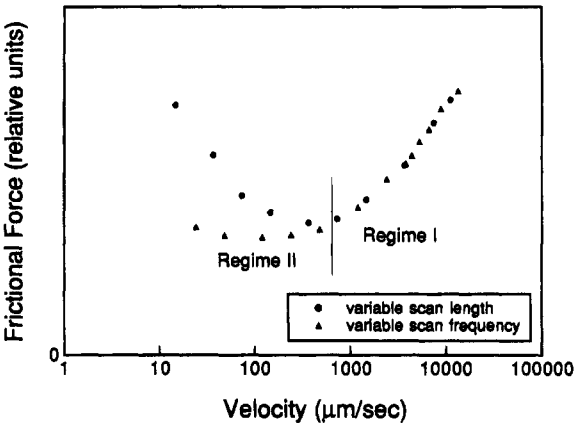

Figure 2. Frictional force as a function of scanning velocity. The velocity was varied via scan length (circles), or scan frequency (triangles). The strictly velocity-dependent domain is designated "regime I"; data differing for variable scan length and frequency comprise "regime II".

The scan velocity is equal to 2 × (scan length) × (scan frequency) and thus was varied via independent variables of scan length (0.005–150 μm) or scan frequency (0.1–55 Hz); a total velocity range of 0.004–16,500 μm/s was investigated. (Lower velocities, reached by further decreasing the scan length, did not produce sliding friction in general.) Up to five friction-loop cycles were averaged per value of velocity, depending on the signal-to-noise ratio at the selected scanning conditions. The contact force was varied by changing the vertical cantilever deflection maintained during scanning. "Force-displacement" measurements, i.e., vertical cantilever deflection as a function of vertical sample displacement toward and away from the surface, were taken to evaluate the contact force. This is given by the sum of the "adhesive" load, quantified from the maximum cantilever deflection toward the sample during withdrawal, and the applied load (positive or negative), specified by the value of cantilever deflection maintained during lateral scanning.

For all data presented here except that in Figure 2, we employed SFM tips which were hydrophobized prior to use

(22) McCrum, N. G.; Read, B. E.; Williams, G. *Anelastic and Dielectric Effects in Polymeric Solids*; Wiley: London, 1967; p 617.

(23) Curme, H. G. In *The Theory of the Photographic Process*, 4th ed.; Mees, C. E. K., James, T. H., Eds.; MacMillan Publishing Co.: New York, 1966; pp 45–71.

employing well-established methods.[24] It was found that these tips were less susceptible to spurious gelatin adsorption during scanning (gelatin accumulation being indicated by a tip–sample adhesive force of increasing magnitude and variability[7]). Careful characterization, however, revealed only minor quantitative differences in frictional data collected with commercial, hydrophobized, and gelatin-contaminated tips. These differences were completely irrelevant to the purposes of the present study; however, ongoing work suggests that tip modification in general may be utilized to "tune" the measurement to particular types of molecular relaxations. In particular a very "blunt" gelatin tip, which accumulates during repeated scanning of unstable gelatin films,[25] exhibits a relatively large frictional interaction at high scanning velocities on the gelatin films presently studied. We used such a tip to collect the data in Figure 2, because these data better illustrate *methodological* differences between variable scan frequency and variable scan length; insights specific to gelatin will be discussed in another article.

3. Results and Discussion

3.1. Velocity Dependence of Frictional Force: Phenomenology. In Figure 2 we plot frictional force as a function of scanning velocity on a gelatin film prepared from 10^{-3} wt % aqueous solution, employing a blunt gelatin tip at a contact force of several hundred nanonewtons (reflecting a large adhesive force, i.e., contact area). The velocity was varied via scan length (circles) or scan frequency (triangles) from high velocity to low. At each velocity data collection began after several scan cycles had been executed; the reason for this will be discussed below. Figure 2 illustrates a general result: (1) strictly velocity-dependent frictional force at high velocities (down to the 100–1000 μm/s decade), and (2) data which differ for variable scan length and scan frequency at lower velocities. We designate the first type of system response as "regime I" and the second as "regime II". We observed these two regimes of behavior on all films independent of the nature of the tip and the concentration of the solution from which the films were prepared.

We investigated whether the friction measurement was *perturbing* the system in regime II, by monitoring the frictional force during repeated scanning. Typically this was performed as follows: (1) at a given location the sample was first retracted from the tip; (2) the sample was raised (via the piezoelectric transducer) while scanning back and forth in the noncontact regime at a frequency of 0.5 Hz in y-disabled mode, until contact was achieved at a designated contact force; (3) this vertical movement was timed to yield nearly a complete left-to-right/right-to-left friction loop in the first cycle; (4) the first and subsequent friction loops were captured and frictional force values calculated for each loop (ignoring any data points collected prior to contact).

We examined several different scan lengths (velocities) and contact forces (F_c); typical frictional force data are presented in Figure 3 for $X = 2$ μm and $F_c \approx 100$ nN (circles), $X = 2$ μm and $F_c \approx 160$ nN (triangles), and $X = 5$ μm and $F_c \approx 160$ nN (squares). The measurement was performed at five locations and the raw data were averaged at each scan loop number. A monotonic rise in friction during repeated scanning is seen; this is particularly notable during the first several scan loops. The rising friction is more significant at $X = 2$ μm compared to $X = 5$ μm and at $F_c = 160$ nN compared to 100 nN. The above observations apply when scanning in regime II; no change in friction with repeated scanning was observed in regime I. Thus we assign regimes I and II to nonperturbative and perturbative scanning conditions, respectively. In either case, before/after image comparisons revealed no topographical modifications (i.e., wear) in the repeatedly-scanned region.

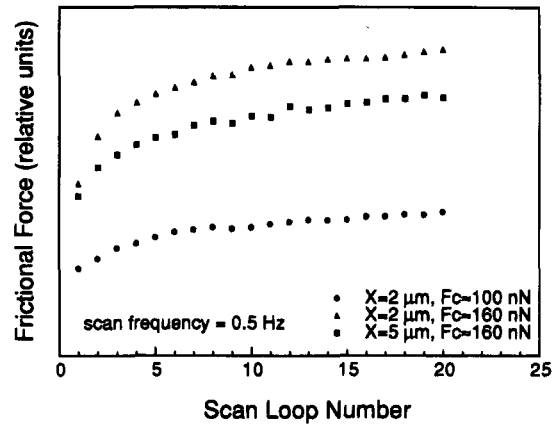

Figure 3. Frictional force versus scan loop number following the establishment of tip-sample contact. Circles correspond to scan length $X = 2$ μm and contact force $F_c \approx 100$ nN, triangles to $X = 2$ μm and $F_c \approx 160$ nN, and squares to $X = 5$ μm and $F_c \approx 160$ nN. Scan loops were repeated at a scan frequency of 0.5 Hz. This was performed at five locations, and the raw data were averaged at each scan loop number.

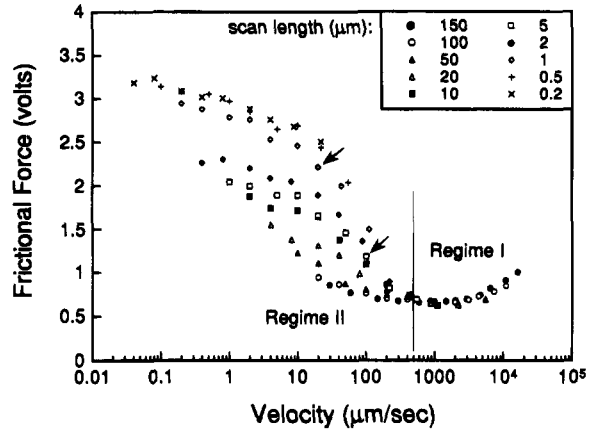

Figure 4. Frictional force versus velocity data collected varying the scan frequency as the independent variable and the scan length parametrically as indicated, each symbol corresponding to a particular scan length. Measurements were performed as a function of decreasing scan velocity, and at each velocity the data collection began after executing at least three scan loops.

We systematically measured frictional force (F_f) versus velocity (v) at a set of lengths, varying the scan frequency as the independent variable. In all such measurements reported in this study, frictional forces were measured as a function of *decreasing* scan velocity. At each velocity the data collection began after executing at least three scan loops. This procedure ensured that plotted data in regime II were essentially *steady state values*: by gradually decreasing the scan velocity, perturbative effects increased only slightly with repeated scanning, in comparison to the dramatic increase seen upon jumping into contact at strongly perturbative conditions (Figure 3). Representative plots for a film prepared from 1 wt % solution are shown in Figure 4 for ten different scan lengths spanning nearly 3 orders of magnitude (scan length = $X = 0.2$–150

(24) This involved exposure of commercial Si_3N_4 tips (which in air have developed a SiO_2 surface layer) to an oxygen plasma followed by hexamethyldisilazane (HMDS) to yield tips terminated by a large number of methyl groups. See Hertl, W.; Hair, M. L. *J. Phys. Chem.* **1971**, *75*, 2181–2185.

(25) Such films result from rapid drying, following a film preparation which is otherwise identical to that used in the present study. The stability of these films (which apparently reflects the extent of gelation) increases over a period of days until the film behavior is qualitatively indistinguishable from that presently described. The characteristics of the unstable films will be reported in more detail in another article.

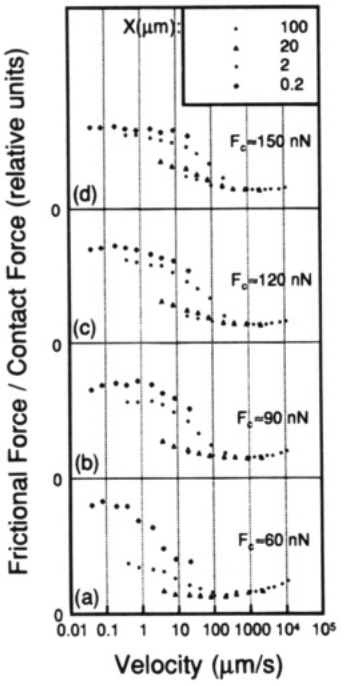

Figure 5. Velocity dependence of the ratio of frictional force to contact force. Contact forces were (a) 60, (b) 90, (c) 120 and (d) 150 nN, and scan lengths 100 μm (circles), 20 μm (triangles), 2 μm (squares), and 0.2 μm (diamonds).

μm), at a contact force of $\approx$90 nN. Above the velocity $v \approx 500$ μm/s the data are essentially scan-length independent, while below that velocity they differ substantially at different scan lengths.

With decrease of the scan velocity in regime II the frictional force typically increases immediately, during the first portion of the first scan loop, indicating a real dependence on scan velocity. Measurements at different scan length/frequency combinations corresponding to the *same* scan velocity revealed *no systematic difference in friction during the first half of the first scan loop;* however, greater friction at higher scan frequencies (and correspondingly smaller scan lengths) was systematically observed after multiple loops had been executed. Moreover, at strongly perturbative scanning conditions and with repeated scanning, the friction loop often was observed to expand vertically (top and bottom) near the left and right ends of the scan loop relative to the middle portion. All of these observations imply that at a particular scan velocity in regime II, a reduction in *time between tip visitations* yields higher frictional forces of magnified *cumulative* effect.

The above observations further suggest that something akin to local heating may occur in regime II. One way to investigate this is to increase the contact force F_c; this should increase F_f and thus the amount of frictional heating. Figure 5 shows the velocity dependence of the ratio F_f/F_c (the coefficient of friction) on a film prepared from 1 wt % solution. Contact forces of (a) 60, (b) 90, (c) 120, and (d) 150 nN were investigated at four scan lengths: $X = 100$ μm (circles), 20 μm (triangles), 2 μm (squares), and 0.2 μm (diamonds). Each relationship $F_f(v,X_i)$, where indices i denote different scan lengths, changes to some extent with increasing contact force. In all cases we observe that with decreasing velocity the frictional force eventually increases substantially (in regime II) and seems to reach a peak. With increasing contact force the trend is to push this peak to higher velocity, i.e., to increase the characteristic rate at which more dissipative behavior is observed. We will discuss the correspondence between frictional heating and dissipative rates in section 3.3.

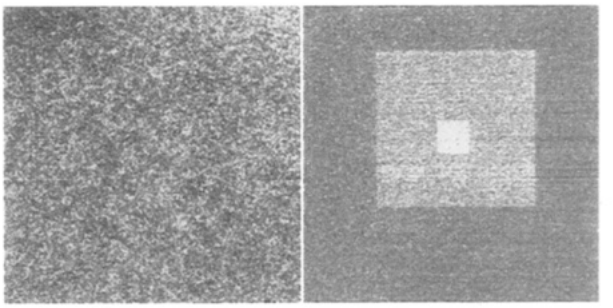

Figure 6. A 10 $\times$ 10 μm topography/friction image (left/right) of 1 $\times$ 1 μm and 5 $\times$ 5 μm regions initially raster scanned in regime II. Brighter regions correspond to higher elevation or frictional force.

3.2. Spatial Distribution of Frictional Forces: Phenomenology. Thusfar we have considered the *average* sliding frictional force measured during complete friction-loop cycles. But SFM clearly can tell us more; in contrast to traditional tribological or deformational probes, SFM can be used to probe friction *locally* on the scale of the tip–sample contact area, as small as $\approx$10 nm^2 on the films investigated here.[7] Thus we can *image variations* in frictional dissipation across the film, including the effects of perturbative scanning.[7] On a film prepared the same as those corresponding to Figures 4 and 5, 1 $\times$ 1 μm and 5 $\times$ 5 μm regions were raster scanned once perturbatively (regime II) at $v = 20$ and 100 μm/s, respectively. The state of the film during these processes was *approximately* consistent with those data points in Figure 4 denoted by arrows. The affected regions were then imaged at $X = 10$ μm and $v = 200$ μm/s, and at *reduced* contact force (which placed the system slightly into nonperturbative regime I). The result is shown in the topography/friction image (left/right) of Figure 6. Brighter regions correspond to higher elevation or frictional force. The friction image displays a 1 $\times$ 1 μm region of greatly-elevated friction and a 5 $\times$ 5 μm region of moderately-elevated friction. The results in Figure 6 are representative of all such observations: increasingly-elevated residual friction in regions scanned further into regime II. No residual effects were observed for scanning in regime I. Remarkably, *no corresponding topographic differences were observed in any region*; this was also true for images taken at higher resolution than in Figure 6.

Changes in frictional character with elapsed time were negligible on the scale of the time required to prepare and image perturbed regions like those in Figure 6. Thus the greater friction in the 1 $\times$ 1 μm region, compared to 5 $\times$ 5 μm, is seen independent of the order in which the regions were scanned. (An observed slow time evolution will be discussed at the end of this section.) Electrostatic charging in the perturbed regions, if occurring, could provide an additional attractive loading force and thereby an increased frictional force. To account for the observed frictional increase, this electrostatic attraction would be easily visible in force-displacement measurements as a dominant contribution to the overall tip–sample attractive force. We did *not* observe an electrostatic contribution, nor any increased tip–sample attraction of any sort, in force-displacement measurements on the perturbed regions.

To interpret the results in Figure 6 requires a more quantitative understanding of friction images. In Figure 7 we present representative topography/friction images (left/right) of a 5 $\times$ 5 μm region of a gelatin film prepared

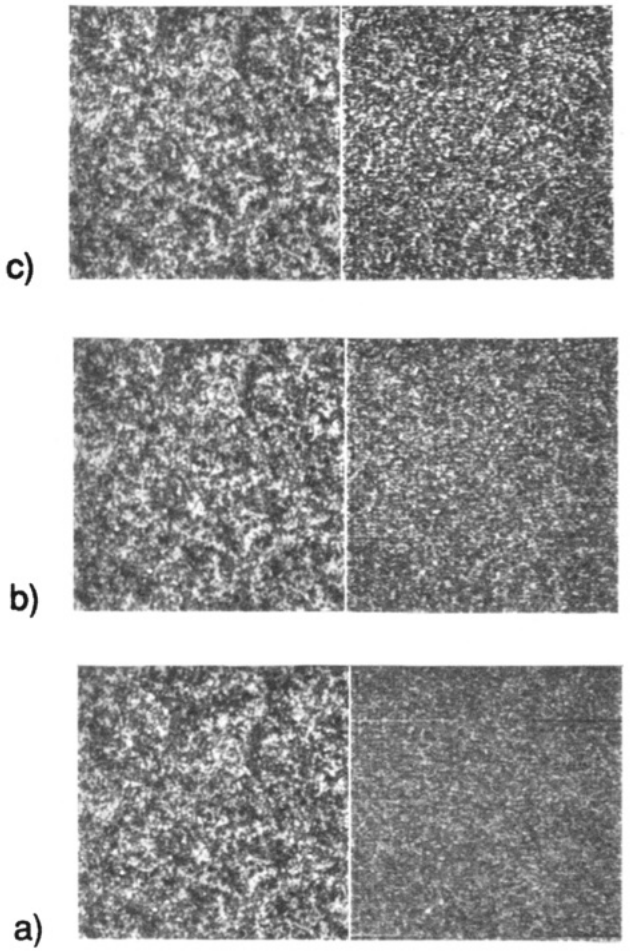

Figure 7. Representative topography/friction images (left/right) of a $5 \times 5\,\mu$m region of a gelatin film collected consecutively (in regime II) at (a) $F_c \approx 60$ nN, (b) $F_c \approx 120$ nN, and (c) $F_c \approx 180$ nN. The contrast range of each friction image is zeroed to its mean value across the image.

from 1 wt % solution. Images a, b, and c were collected consecutively at $F_c = 60$, 120, and 180 nN, respectively, and at $v = 100\,\mu$m/s. The contrast range of each friction image is zeroed to its mean value across the image. Both topographic and frictional images are "granular" in character, reflecting a contact area substantially larger than the fibrous structural components of the film.[7,26] With increasing contact force we discerned a slight decrease in topographic resolution (quantified in profile examinations and roughness analysis), reflecting a larger contact area, but otherwise no differences; the friction images on the other hand display a markedly increased variation of frictional force (contrast).

Imaged variations in friction greatly exceeded the noise. This was seen during successively magnified imaging, wherein the frictional "grains" increased in size. Moreover the location of "grains" of greater or lesser friction was fairly reproducible, indicating a real spatial distribution of friction, not a distribution varying randomly from one image to the next. Pixel-by-pixel statistical analysis revealed a finite correlation in each image pair between the position of topographic and frictional "grains" but no correlation between the *slope* of topography and the magnitude of frictional force.[27] We therefore interpret the friction images as maps of real variations in frictional *dissipation* across the film, i.e., not corrugation-derived variations (conservative forces) which in general contribute to cantilever torsion.[7,15] (Occasional protrusions imaged at some locations, with slopes at least a factor of 10 greater than those observed in Figure 7, were indeed large enough to affect cantilever torsion measurably.)

(26) Djabourov, M. *Contemp. Phys.* **1988**, *29*, 273–297.

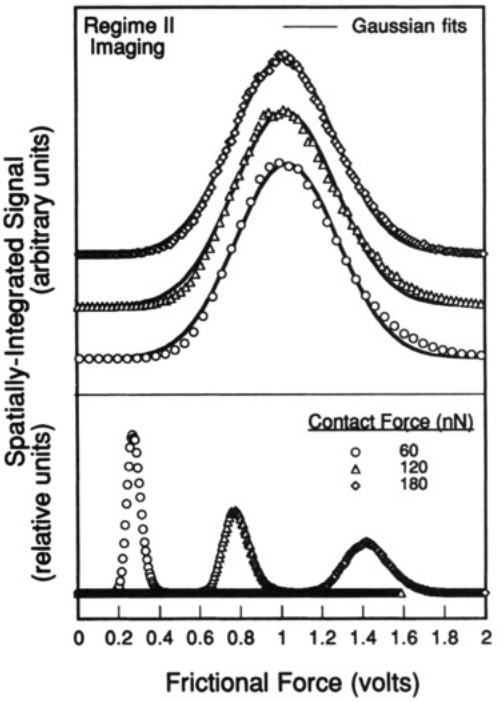

Figure 8. (Bottom panel) "Friction spectroscopy" data, i.e. histograms of the number of image pixels in incremental frictional force intervals, corresponding to $3 \times 3\,\mu$m subregions of the images in Figure 7 collected (in regime II) at contact forces of 60 nN (circles, 7a), 120 nN (triangles, 7b), and 180 nN (diamonds, 7c). (Top panel) Same data with abscissa and ordinate expanded (by varying amounts) to compare histogram *shapes*. Gaussian-lineshape fits are shown as lines.

The images in Figure 7 were obtained at scanning conditions in regime II; increasing the contact force pushes the system further into this perturbative regime (see Figure 5). The scanning conditions for each image were as follows: (a) barely into regime II; (b) further in but corresponding to the rapidly rising portion of $F_f(v)$; (c) well into regime II, closer to the maximum of the frictional peak. We quantified the friction images in Figure 7 as histograms to construct a *distribution function* of frictional dissipation. We subdivided the frictional force range into 256 intervals and counted the number of pixels contained in each friction interval, over the same $3 \times 3\,\mu$m subregion of each image (approximately $300^2 = 90\,000$ pixels each). Each data point in Figure 8 represents the "spatially-integrated signal", i.e. the number of image pixels counted in a frictional force interval; we call this analysis "friction spectroscopy". In the bottom panel we see that at contact forces of approximately 60 nN (circles), 120 nN (triangles), and 180 nN (diamonds), respectively, we obtain increasingly broad histograms centered at higher frictional force. (The zero of frictional force was determined from friction loop data.) In the top panel we examine the same data with abscissa and ordinate expanded (by varying amounts)

(27) This involved computing the correlation function

$$\chi = \frac{1}{N}\sum_i \frac{(A_i + B_i)^2}{(A_i^2 + B_i^2)} - 1$$

where A_i and B_i are the appropriately-scaled frictional force and height at the ith pixel, summed over N pixels. Values of $\chi = 1$, 0, and -1 correspond to completely correlated, uncorrelated, and anticorrelated data, respectively.

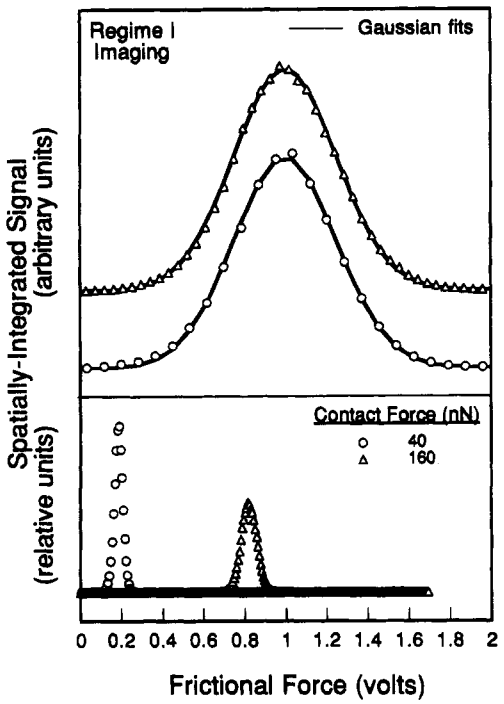

Figure 9. (Bottom panel) Friction spectroscopy data corresponding to 3 × 3 μm subregions of images similar to those in Figure 7, but on a more mature gelatin film at scanning conditions in regime I. Contact forces were ≈40 nN (circles) and ≈160 nN (triangles). (Top panel) Same data with abscissa and ordinate expanded (by varying amounts). Gaussian-lineshape fits are shown as lines.

to compare histogram *shapes*. We superimpose as lines the results of fits to Gaussian lineshapes of the form

$$P(F_f) = A \exp\left[\frac{-(F_f - F_f^\circ)^2}{2\sigma^2}\right]$$

with fitting parameters A, F_f°, and σ, which determine the height, position and width of each peak, respectively. A fairly good fit is obtained at $F_c \approx 180$ nN but not at $F_c \approx 60$ or 120 nN, reflecting clearly asymmetric lineshapes in the latter cases. Histogram symmetry did not change qualitatively with repeated scanning of the same region, although some quantitative changes were apparent.

Figure 9 corresponds to 3 × 3 μm subregions of friction images similar to those in Figure 7, collected on the same day with the same tip at the same velocity, but on a more mature gelatin film at scanning conditions in regime I, at $F_c \approx 40$ nN (circles) and 160 nN (triangles). The histograms in the bottom panel display shifting and broadening with increasing F_c, but not nearly as much as the regime II case (Figure 8) for similar contact forces. The top panel compares the same data with expanded abscissa and ordinate and superimposed Gaussian fits (lines). Here we obtain good fits of both histograms, reflecting symmetric lineshapes.

Figures 8 and 9 are representative of the contact-force and scanning-condition dependence of all friction spectroscopy data we have analyzed thus far. It seems that increased deformation (via a larger F_c[28]) not only magnifies the average frictional dissipation but also yields a greater "dispersion" of dissipative events.[29] Friction lineshapes were generally symmetric for scanning conditions in regime I, asymmetric upon entering regime II, and nearly symmetric for conditions well into Regime II. Thus to a first approximation the distribution of dissipative character is described by Gaussian statistics, but moderately-perturbative scanning seems to yield a statistical bias toward greater dissipation.

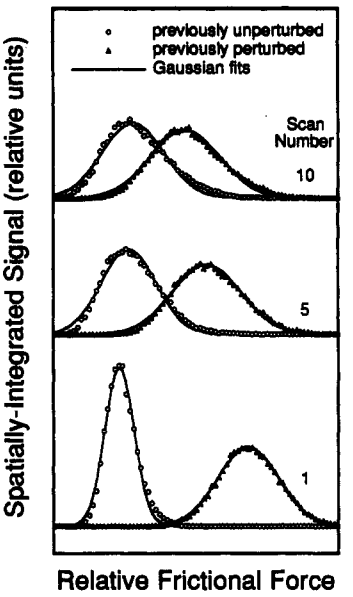

Figure 10. Friction spectroscopy data corresponding to successive 5 × 5 μm images of 2 × 2 μm regions previously scanned well into regime II. The histograms correspond to the first (bottom), fifth (middle), and tenth (top) images collected following termination of the 2 × 2 μm raster scanning. Histograms of the 2 × 2 μm scan-perturbed region are plotted as triangles, and those from a same-size subregion of the previously-unperturbed region are plotted as circles. Gaussian fits are shown as lines.

We applied friction spectroscopy to investigate more quantitatively the *residual* effects of perturbative scanning qualitatively illustrated in Figure 6. We collected successive 5 × 5 μm images of 2 × 2 μm regions initially scanned well into regime II, to monitor changes in histogram character with repeated scanning at more moderate conditions. Representative histograms are shown in Figure 10 corresponding to the first (bottom), fifth (middle), and tenth (top) images collected following termination of the 2 × 2 μm raster scanning. Histograms of the 2 × 2 μm scan-perturbed region are plotted as triangles, while those from a same-size subregion of the (previously unperturbed) surrounding film are plotted as circles; Gaussian fits are superimposed as lines. The asymmetric lineshape for the low-friction region in scan 1 is consistent with scanning conditions slightly into regime II. The high-friction region yields an initially broader, essentially symmetric lineshape, similar to that obtained from the image in Figure 7c which was collected at scanning conditions well into regime II. With repeated imaging the low-friction component shifts a bit to higher frictional force and broadens; the high-friction component shifts to lower friction and becomes asymmetric. We did not attempt to determine the number of raster scans required to yield identical histograms but have noted that repeated scanning over such initially-dissimilar friction regions eventually yields indistinguishable regions. In sum, upon changing scanning conditions the lineshapes initially depend on the *preceding* state of the system, but

(28) Israelachvili, J. N. *Intermolecular and Surface Forces*, 2nd ed.; Academic Press: San Diego, CA, 1991; p 450.

(29) This is consistent with a trend observed in Figure 5: the *decrease* of frictional force as a function of decreasing velocity below 1 μm/s (e.g. Figure 5b) often was not observed at higher F_c (e.g. Figure 5d), suggesting a broader distribution of dissipative events in the latter case.

with repeated imaging the histograms approach one another in position and lineshape to reflect the scanning conditions during imaging.

To examine the intrinsic *time evolution* of dissipative film character, we have modified 2 × 2 μm regions, retracted the sample and waited a variable length of time, and then reestablished contact and imaged (once). We monitored an evolution of friction in the modified region which was similar to that of Figure 10, but instead as a function of elapsed *time* between modification and imaging. This evolution was very slow, however: a 10–30 min wait yielded changes similar to *one* raster scan, the latter requiring only ≈30 s. Hence with elapsed time the film tends to return to a less dissipative state, but continuous scanning during the same period speeds this transition by more than a factor of 10.

3.3. Molecular Interpretations. Gelatin at room temperature is a glassy (nonequilibrium) network containing two distinct molecular structures: (1) entangled, randomly-oriented (amorphous) polypeptide strands, and (2) the same strands wound together as triple-helical ("crystalline") physical cross-links.[26] The latter are rigid linear structures, held together by relatively strong hydrogen bonds, and may collect into larger fibrils containing a number of triple-helical units.[30] In regions where the former predominate, rotations about covalent bonds along the polypeptide main chain are easily activated at room temperature but are hindered by steric restraint and random hydrogen bonds. In nominally-dry films steric interactions are considerable; in order for a "conformer" (the smallest unit of rotation[31]) to complete a rotation, cooperative rotations by several nearby conformers are necessary (on the same and/or neighboring strands). Cooperative relaxation of conformers is the source of relaxation times which are much larger than predicted from a single relaxation: the composite relaxation time essentially goes as $\exp(E_a z/kT)$, where E_a is the activation energy for a single rotation and z is the number of conformers which must cooperate for a single event.[31] Variations in the size of relaxational domains, i.e. the number of conformers "meshed" together, result in a broad distribution of relaxation times.[22,31–33]

An applied stress deforms a polymer resulting in higher-energy molecular conformations, followed by relaxations to more favorable conformational states. The degree of relaxational cooperativity depends strongly on temperature: the higher the temperature, the more extensive the deformation and subsequent relaxation. Well into the glassy regime the extent of molecular relaxation is small; typically these "secondary" relaxations are thought to involve side groups or very small segments of the polymer main chain.[22,31–33] Higher temperatures activate relaxations involving a larger number of conformers; these motions can yield a net "stretching" of polymer strands and hence are associated with the glass-to-rubber transition.

For polymers it is known from conventional (macroscopic) characterization that the velocity-dependence of frictional force is very similar to the rate-dependence of $\tan(\delta)$ where δ is the complex phase of viscoelastic moduli in dynamic measurements.[22,32] This relationship generally displays several broad peaks corresponding to different classes of molecular relaxation, each class encompassing a sizable range of relaxation times.[22,32] Typically three broad relaxational peaks are observed in $\tan(\delta)$ viscoelastic measurements of polymers as a function of increasing temperature or time, prior to the melting transition.[22] The first two involve secondary relaxations conventionally labeled γ and β, while the last reflects rubbery or α relaxations.

At conventional measurement rates the glass-to-rubber transition in gelatin is interpolated as $T_g \approx 40–70$ °C for water content in the 12–17% range[34] (corresponding to RH = 30–60%[23]). At the same rates secondary relaxations therefore should peak below room temperature.[22] We assign the elevated friction at low velocities and small dimensions in Figures 2, 4, and 5 to the glass-to-rubber transition peak, and rising friction at the highest velocities to secondary relaxations. Perturbative (regime II) scanning apparently shifts the the onset of rubbery behavior to higher velocity (in the scanned region). We have observed preliminarily that higher ambient humidity (i.e. higher water content in the gelatin[23]) also shifts this transition to higher rate, consistent with conventional measurements.[22,34] Inconsistent with the behavior of *secondary* relaxations is a lack of a decrease in height with aging.[35]

The heat capacity of a glass is understood to contain a substantial configurational component in addition to the ordinary vibrational (Debye) component.[35,36] Scanning in regime II apparently leaves many gelatin molecules in higher-energy conformational states, from which a broader spectrum of relaxations of greater mean energy can occur (Figure 8, bottom panel). Achieving higher-energy states presumably requires crossing larger activation-energy barriers, which at room temperature (and in the absence of perturbation) restrict accessible state space to nearly-degenerate conformational states lower in the *hierarchy* of glassy configuration space.[37–39] Repeated scanning at highly-perturbative conditions eventually yields a broad, steady-state distribution of conformations with a stable mean relaxational dissipation (Figure 3). Conformational energy is not shared readily with the larger system; an excess remains confined to a region (Figure 6) as "athermal" energy.[36] Left alone, this subsystem will slowly relax to its "ground state" conformational distribution.[40] Alternatively, scanning at less perturbative conditions supplies energy to speed the relaxational process. Relaxations to lower-energy conformations tend to win out over the replenishment of higher-energy states; a new steady state distribution of conformations is attained from which high-energy relaxations do not take place, leaving more moderate dissipative events (Figure 10, top right peak). Identical scanning of previously unperturbed regions asymptotically yields the same distribution, but

(30) Tomka, I.; Bohonek, J.; Spühler, A.; Ribeaud, M. *J. Photogr. Sci.* **1975**, *23*, 97–103.
(31) Matsuoka, S. *Relaxation Phenomena in Polymers*; Oxford: New York, 1992; p 322.
(32) Aklonis, J. J.; MacKnight, W. J. *Introduction to Polymer Viscoelasticity*, 2nd ed.; Wiley: New York, 1983; p 295.
(33) *Molecular Dynamics and Relaxation Phenomena in Glasses*; Dorfmüller, T., Williams, G., Eds.; Lecture Notes in Physics; Springer-Verlag: Berlin, 1987; Vol. 277, p 218.
(34) Marshall, A. S.; Petrie, S. E. B. *J. Photogr. Sci.* **1980**, *28*, 128–134.
(35) Johari, G. P. In *Molecular Dynamics and Relaxation Phenomena in Glasses*; Dorfmüller, T., Williams, G., Eds.; Lecture Notes in Physics; Springer-Verlag: Berlin, 1987; Vol. 277, p 90–112.
(36) Austin, R. H. In *Lectures in Complex Systems*; Nadel, L., Stein, D., Eds.; Addison-Wesley: New York, 1993; Vol. 5.
(37) Palmer, R. G.; Stein, D. L.; Abrahams, E.; Anderson, P. W. *Phys. Rev. Lett.* **1984**, *53*, 958–961.
(38) Blumen, A.; Klafter, J.; Zumofen, G. *J. Phys. A* **1986**, *19*, L77–L84.
(39) Frauenfelder, H. In *Physics in Living Matter*; Baeriswyl, D., Droz, M., Malaspinas, A., Martinoli, P., Eds.; Lecture Notes in Physics; Plenum Press: New York, 1991; Vol. 284.
(40) This distribution itself changes with time: for gelatin, no true ground state is reached until the material has regained fully the tertiary and higher-order structures of the collagen protein from which it is derived (ref 23). (Extrapolation of the logarithmic experimental trends in ref 26 suggests that this would require times on the order of 1 Myear!)

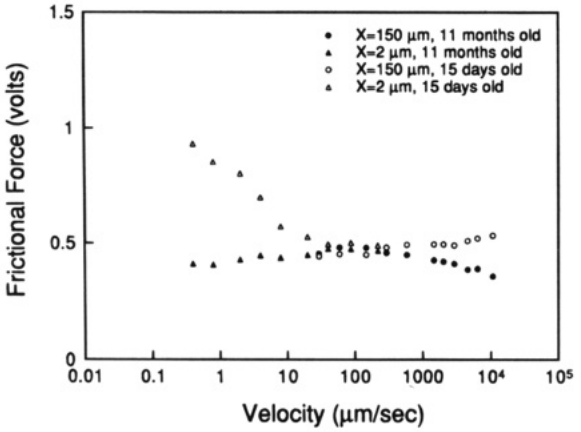

Figure 11. Frictional force versus velocity at scan lengths of $X = 150$ μm (circles) and 2 μm (triangles) on gelatin films of different ages: 11 months (solid symbols) and 15 days (open symbols).

approaching from below rather than above (Figure 10, top left peak).[41]

Characterization with conventional methods provides no direct information about either the spatial distribution or the energy dispersion of molecular relaxations. Our results suggest that (1) friction images on a stable polymer network are essentially real-space maps of molecular relaxation across the film and (2) friction spectroscopy quantifies the energy dispersion of relaxations. Note that while this dispersion clearly is a function of the velocity regime examined, it may also depend on the variability of chemical interactions with the tip, molecular orientations relative to the scan direction, etc.

3.4. Application of Molecular Interpretations. Quantitative comparison of results for gelatin films of different water content,[42] or prepared from different-concentration solutions, or dried, hardened or aged differently, has suggested the utility of $F_f(v)$ measurements to characterize molecular coupling. We defer an in-depth presentation of these results to another article. It is suitable to present here one result, however, as it aids in illustrating the usefulness of our method. Generally we have found that with aging of gelatin films, the low-v relaxation shifts to lower v and regime II behavior does not occur at $X > 1$ μm. Concomitantly the frictional rise at high velocity diminishes and eventually disappears. These findings are exemplified in Figure 11, a comparison of results with $X = 150$ μm (circles) and 2 μm (triangles) on films 11 months (solid symbols) and 15 days (open symbols) old, taken on the same day with the same tip at the same contact force (≈70 nN). The data imply the presence of a broad intermediate class of relaxations centered at about 100 μm/s, fully visible only in aged films following the disappearance of both slower (rubbery) and faster relaxations.

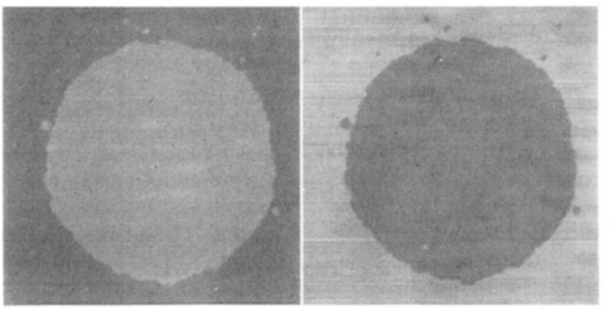

Figure 12. A 35 × 35 μm topography/friction image (left/right) of a rather large, low-friction island (and some smaller ones) commonly observed on the two-phase gelatin films reported in ref 7.

Preclusion of relaxations presumably is due to reduced conformational freedom,[22,31-33] which may reflect increased cross-linking/entanglement or reduced specific volume with aging, familiar concepts in gelatin and polymer science: (1) the triple-helical content in gelatin films, and hence the level of physical cross-linking, is known to increase as the logarithm of time on an extremely long time scale,[26] and (2) reduced specific volume with age is a characteristic of many glassy materials.[35] To identify and separate such effects firmly, however, requires systematic studies of simpler polymeric systems (in progress).

In a recent study[7] we observed a low-friction minority phase of gelatin present primarily as islands on top of the high-friction network film presently investigated. A 35 × 35 μm topography/friction image (left/right) of a rather large island (and some smaller ones) is shown in Figure 12, taken at $v = 240$ μm/s and $F_c \approx 50$ nN. This phase was interpreted as intramolecularly-folded triple-helical ("crystalline") gelatin.[26] The absence of noncrystalline "stretchable" domains should preclude rubbery behavior and result in a direct glass-to-melt transition with heating.[43] Hence the molecular understanding of friction proposed in section 3.3 can be checked for consistency with our past interpretation of low-friction islands as folded moieties.

Figure 13 contains friction-versus-velocity data simultaneously collected on these moieties and the high-friction network. The velocity was varied via the scan length at scan frequencies of 55 Hz (open circles) and 5 Hz (open triangles) on the high-friction network and at 55 Hz on a low-friction island (closed circles). A frictional rise at smaller scan lengths, characteristic of the onset of rubbery behavior, is observed on the network but not on the island. We have observed that upon increasing the contact force above a critical value, the scanned portions of the low-friction islands simply disappear.[7] Apparently these regions are heated sufficiently to liberate the gelatin molecules completely, i.e. to induce the melting transition. Thus our molecular interpretations of the past and present studies seem consistent.

In polymers, viscoelastic spectra shift to faster rates with increasing temperature, reflecting shortened conformational relaxation times (whose temperature dependence is contained in rate constants for sterically-restrained rotations about chemical bonds[31]). Equivalently, a tan(δ)-versus-temperature spectrum shifts to higher temperature with increasing rate. The underlying physics

(41) A speculative but plausible explanation of frictional lineshape symmetry is as follows. Scanning conditions in regime I correspond to an equal *a priori* probability of populating conformations within a small "sphere" of hierarchical state space (refs 37–39); in the vocabulary of statistical mechanics such an assembly of states would be *ergodic*. (See Palmer, R. G. *Adv. Phys.* **1982**, *31*, 669–735.) As a result there is an equal probability for relaxations above and below some mean dissipational value; this is manifest as a Gaussian friction-spectroscopy lineshape. When slightly into regime II, the partial population of a higher-energy class of conformations skews the distribution toward greater dissipation (friction). At this point equal *a priori* probability of state population may not hold, i.e. there may be *broken ergodicity* in a partially-accessible region of state space. (Broken ergodicity with respect to *all* of state space always applies to glassy systems on laboratory time scales.) With increasingly perturbative scanning, equal *a priori* probability of state population within the accessible conformation space again may hold approximately (state space essentially ergodic), so that the "spectrum" of relaxations approaches a symmetric distribution.

(42) Gelatin is understood to contain 10–20% water by weight when equilibrated with air at 20–80% relative humidity (RH). See ref 23. Hence the films examined (RH = 30–60%) presumably contained ≈12–17 wt % water depending on the (monitored) ambient humidity.

(43) Yannas, I. V. *J. Macromol. Sci. C* **1972**, *7*, 49–104.

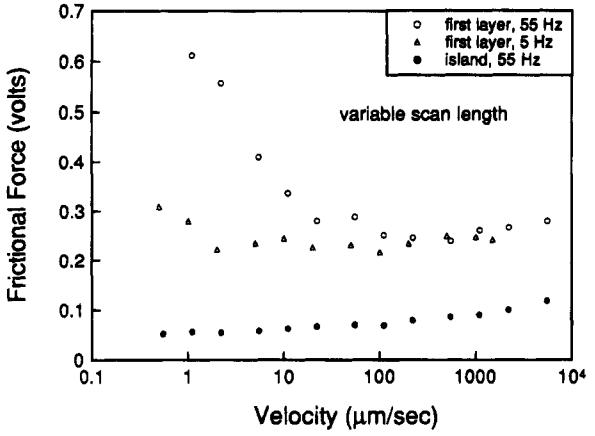

Figure 13. Frictional force versus velocity data simultaneously collected on a low-friction island like that in Figure 12 and on the high-friction film surrounding the island. The velocity was varied via the scan length at scan frequencies of 55 Hz (open circles) and 5 Hz (open triangles) on the high-friction film and at 55 Hz on a low-friction island (closed circles).

is known as the time–temperature correspondence principle. In conventional measurements it is experimentally difficult to span the entire viscoelastic spectrum by varying only the rate. A set of data may be collected as a function of rate and repeated at multiple temperatures; data sets then can be shifted along the abscissa relative to one another and superimposed to construct a "master curve" which characterizes the broader viscoelastic spectrum.[32]

We investigated whether such methods might be applied to our data. We postulate that at a given scan length a particular dynamic equilibrium of energy transfer results, which *in effect* is equivalent to placing the subsystem (scanned region) at an elevated temperature. Then the data sets $F_f(v,X_i)$ collected at different scan lengths X_i can be appropriately shifted relative to one another and superimposed, as if they corresponded to different temperatures. The application of this procedure to data taken on a gelatin film prepared from 1 wt % solution is illustrated in Figure 14. Data sets were collected with F_c = 90 nN and at five scan lengths, X = 150 μm (circles), 20 μm (triangles), 2 μm (squares), 0.2 μm (diamonds), and 0.02 μm (crosses). The raw data are displayed in the bottom panel and the shifted data in the top. In each set taken at X < 150 μm, we multiplied the velocities by different factors (a_X) less than unity to shift the individual sets to lower velocity by varying amounts. Achieving the "master curve" in the top panel also required multiplying the frictional forces by factors (b_X) less than unity. Such vertical shifts in conventional viscoelastic data generally indicate changes in modulus and density associated with a change in temperature.[32] We assign our vertical shifts to softening which increases the severity of deformation, thereby elevating frictional dissipation.

Similar procedures applied to a large number of $F_f(v,X)$ data sets acquired for several gelatin films yield "master curves" qualitatively similar to that in the top of Figure 14. The suggested breadth and separation of the identified "peaks", in decades of rate, are not inconsistent with spectra catalogued for polymers using traditional viscoelastic probes and varying the *temperature* parametrically, as we do the scan length.[22,31] Thus it seems that scanning at a particular size X_i is equivalent *in effect* to thermal equilibration with a heat reservoir of temperature T_i. We are designing SFM experiments which will allow sample temperature to be varied controllably, in order to test this hypothesis directly.

The observation that increasing scan frequency at *fixed* scan length does not increase regime II perturbative effects

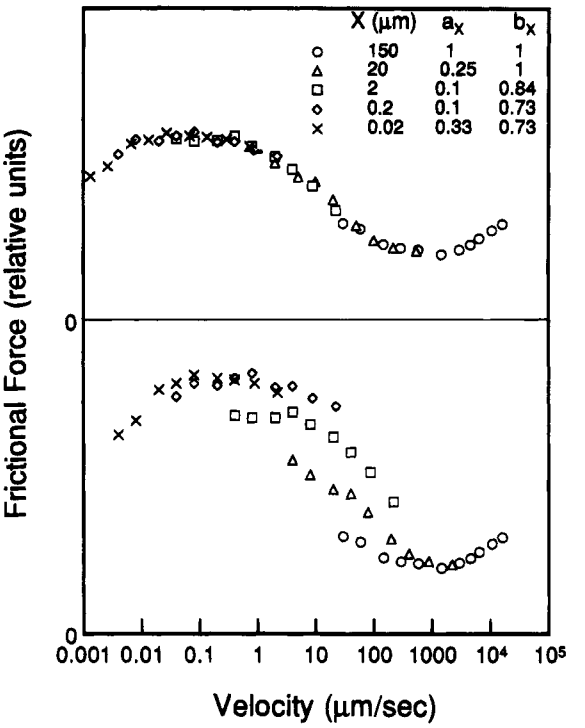

Figure 14. Five sets of frictional force versus velocity data corresponding to scan lengths of X = 150 μm (circles), 20 μm (triangles), 2 μm (squares), 0.2 μm (diamonds), and 0.02 μm (crosses). Unmodified data are displayed in the bottom panel. In the top panel the velocity and frictional force data were multiplied by the factors a_X and b_X, respectively, to yield a consistent trend.

seems puzzling at first sight. The mathematics of the relationship $F_f(v)$ in regime II may provide some insight, however. For $\partial F_f/\partial v$ < 0, decreasing v (via X) increases F_f and thereby the frictional heating; a resulting shift of the relationship $F_f(v)$ to the right further increases F_f, i.e. positive feedback occurs. (Note that the horizontal shift factor a_X in Figure 14 decreases with decreasing X only as long as $\partial F_f/\partial v$ is distinctly negative.) In comparison, increasing the scan frequency (and hence v) at fixed scan length *decreases* F_f. Any increased heating due to faster scan repetition may not shift the $F_f(v)$ relationship far enough to the right to yield a *net* increase in F_f, i.e. positive feedback may not occur.

Conclusions

Measurements of frictional force versus scan velocity (0.004–16500 μm/s) on nominally-dry gelatin films revealed two regimes of behavior: (I) strictly velocity-dependent frictional force at high scan velocities (typically >300 μm/s on newly-prepared films), and (II) a velocity dependence varying sharply for different scan length/frequency combinations at lower velocities. The transition from regime I to regime II occurred at higher velocity when operating at higher contact force or scan frequency, i.e. when depositing energy into the film at a faster rate. Well into regime II the measured frictional force clearly was affected by the measurement itself: repeated scanning yielded increasing frictional force. Moreover a residual high-friction signature subsequently was imaged at the site of regime II scanning, but without corresponding morphological differences. Repeated imaging at less perturbative scanning conditions eventually yielded frictional forces characteristic of these conditions, further indicating that the dissipative characteristics of the film depends strongly on the energy imparted by the scanning process itself (the system is inherently nonlinear). Con-

sistent with the known correlation between friction and viscoelastic dissipation in/on polymers, we assigned the rise in frictional force at the regime I-to-II transition to the onset of molecular relaxations characteristic of the rubbery state. An increasing frictional force at the highest velocities attainable then corresponds to the appearance of a secondary-relaxation peak. The cumulative and residual effects of scanning in regime II were attributed to the population of higher-energy molecular conformations, from which more energy-dissipative relaxations are possible.

Imaged variations in frictional force tens of nanometers in lateral size easily exceeded the noise, were fairly reproducible from one image to the next, and did not correlate with corrugations in the imaged topography; hence they were interpreted as real differences in the energy-dissipative character of different film portions. The distribution of frictional forces sensed over micrometer-scale regions were quantified as histograms of the number of image pixels versus frictional force. To our knowledge this was the first analysis of the *dispersion* of energy dissipation contained in friction force microscopy images and, thus, was termed "friction spectroscopy". The breadth and symmetry of friction spectroscopy lines were characteristic of glassy or rubbery behavior identified in the friction–velocity measurements.

The above fundamental interpretations of FFM were applied preliminarily to assess aging and crystallinity in gelatin films. We conclude that in aged gelatin films the glass-to-rubber transition shifts to lower rates, consistent with conventional understandings of a slow increase in physical cross-linking in gelatin, and decreasing specific volume in polymers in general. Our previous interpretation of low-friction islands as moieties of highly-crystalline, folded gelatin was found to be consistent with a direct glass-to-melt transition implied in friction–velocity and friction–load measurements.

Acknowledgment. Support by the Center for Interfacial Engineering, a National Science Foundation Engineering Research Center, and a grant from E. I. du Pont de Nemours and Co., Inc., is gratefully acknowledged. For hydrophobizing SFM tips we are most grateful to J. F. Evans for supplying his time, equipment, and expertise.

LA950051N